JACS
JOURNAL OF THE AMERICAN CHEMICAL SOCIETY
pubs.acs.org/JACS

Article

Biased Bowl-Direction of Monofluorosumanene in the Solid State

Yumi Yakiyama,* Minghong Li, Dongyi Zhou, Tsuyoshi Abe, Chisato Sato, Kohei Sambe, Tomoyuki Akutagawa, Teppei Matsumura, Nobuyuki Matubayasi, and Hidehiro Sakurai

Cite This: J. Am. Chem. Soc. 2024, 146, 5224−5231

Read Online

ACCESS | Metrics & More | Article Recommendations | Supporting Information

ABSTRACT: A new curved π-conjugated molecule 1-fluorosumanene (**1**) was designed and synthesized that possesses one fluorine atom on the benzylic carbon of sumanene. This compound can exhibit bowl inversion in solution, leading to the formation of two diastereomers, $\mathbf{1}_{endo}$ and $\mathbf{1}_{exo}$, with different dipole moments. Experimental and theoretical investigation revealed an energetical relationship among $\mathbf{1}_{exo}$, $\mathbf{1}_{endo}$, and solvent to realize the various *endo*:*exo* ratios in the single crystals of **1** depending on the crystallization solvent. Significantly, the molecular dynamics (MD) simulations revealed that $\mathbf{1}_{exo}$ positively worked for the elongation of the stacking structure and the final *endo*:*exo* ratio was affected by the relative stability difference between $\mathbf{1}_{endo}$ and $\mathbf{1}_{exo}$ derived by solvation. Such an arrangeable *endo*:*exo* ratio of **1** realized the preparation of unique materials showing a different dielectric response from the same molecule **1** just by changing the crystallization solvent.

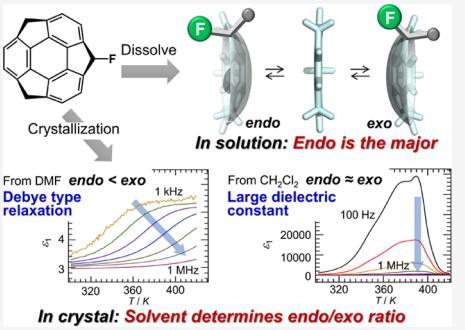

INTRODUCTION

The process of nucleation, the initial step in crystallization, is largely affected by various factors such as temperature, solvent, concentration of the solute, and impurities.[1] These factors significantly affect the molecular arrangements and morphology of the resulting crystals. Understanding these structural aspects is crucial as they are closely linked to the physical properties of crystalline materials. Notably, the contribution of solvents to the nucleation has been investigated recently by combining the experimental approach using ^{1}H NMR and FT-IR spectroscopies and the theoretical one applying density functional theory (DFT) calculations and molecular dynamics (MD) simulations. The outcomes of these studies have unveiled discernible solvent-induced effects on nucleation events in various small aromatic compounds[2−10] and pharmaceutical molecules.[11−14] Despite these advancements, the general rules governing nucleation and subsequent crystallization processes remain elusive.[15−17] Therefore, the control of crystal packings and the physical properties of the crystals remain a challenging issue.

Buckybowls are the partial structures of fullerenes such as C_{60} and are recognized as distinctive molecular components in the realm of new molecular materials. Bowl-to-bowl inversion is one of the most representative and attractive phenomena in buckybowl chemistry. This unique property of the curved-π system affords a variety of structural and physical properties that respond to external environments. Consequently, these buckybowls hold potential applications as the molecular switches responsive to external stimuli.[18] One representative buckybowl, sumanene (**Sum**), also shows dynamic phenomenon involved by its bowl inversion in the solution state (Figure 1).[19,20] **Sum** possesses three benzylic carbons, and their two geminal protons are not geometrically equivalent due to the bowl structure. This characteristic implies that monobenzyl substitution on sumanene potentially gives *endo*- (concave side) and/or *exo*- (convex side) substituted derivatives. The resulting *endo*:*exo* product ratio is affected by the electronic factor, namely, the stereoelectronic effect, as well as the structural factor, mainly the steric hindrance between the substituent and the bowl.[21] For example, OH group substitution exclusively yields the *endo* product, while trimethylsilyl substitution gives only the *exo* product. The above example shows noticeable energy differences between the corresponding diastereomers. Meanwhile, the reaction with comparable *exo* and *endo* populations is also reported if the two diastereomers possess similar energy. In such an occasion, it is expected that other environmental factors such as the temperature, concentration, solvent, and the presence of other additives may affect the final *endo*:*exo* ratio. Especially in the crystalline state, in which small intermolecular interactions afford different types of stabilization effects from that in the solution state, it is unsurprising to observe a disparate *endo*:*exo* ratio.

Recently, our focus has been on studying fluorine-introduced buckybowls,[22−24] especially fluorosumanenes[25−28] from both structural and application viewpoints. The salient feature of these compounds is that they form isostructural

Received: October 12, 2023
Revised: January 5, 2024
Accepted: February 2, 2024
Published: February 20, 2024

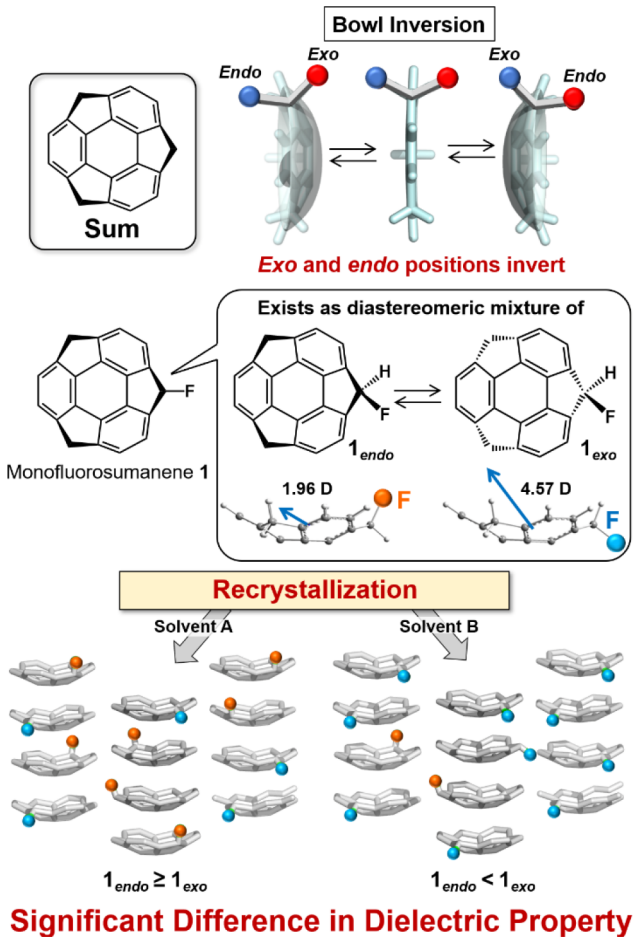

Figure 1. Bowl inversion of **Sum** and the conceptual figure of this work.

single crystals of pristine sumanene.[29,30] Particularly intriguing is the instance of difluorosumanene (**F2-Sum**), where two fluorine atoms are on a single benzylic carbon site. This configuration induces the anisotropic dielectric response due to its strong dipole moment caused by F-introduction.[26] This attribute has been harnessed to create solid solutions with pristine sumanene and change the activation energy of dielectric response depending on the **Sum**:**F2-Sum** ratio.[27] In this context, we further extended our interest to another fluorosumanene family, monofluorosumanene (**1**), which possesses one fluorine atom at the peripheral benzylic carbon. In this paper, we found that **1** was a diastereomeric mixture of its *endo*- ($\mathbf{1}_{endo}$) and *exo*- ($\mathbf{1}_{exo}$) substituted products in solution and solid states. Because of the curved structure of the sumanene skeleton, $\mathbf{1}_{endo}$ and $\mathbf{1}_{exo}$ exhibited distinct electronic structures, leading to different dipole moments (1.96 D for $\mathbf{1}_{endo}$ and 4.57 D for $\mathbf{1}_{exo}$ at B3LYP/6-311+G(d,p)). Noteworthy is that **1** gave the isostructural single crystal packing of **Sum**, and its *endo*:*exo* ratio significantly changed depending on the crystallization solvent from $\mathbf{1}_{endo}$:$\mathbf{1}_{exo}$ = 60:40 to 18:82. This alternation in the *endo*:*exo* ratio directly corresponds to a remarkable difference in the dielectric response of each crystal. In addition, we investigated its mechanism through quantum chemistry calculations and molecular dynamics simulations to find that solvation and intermolecular interactions in the aggregated structure significantly affected the final *endo*:*exo* ratio in the crystals.

RESULTS AND DISCUSSION

Monofluorosumanene (**1**) was synthesized from direct fluorination of previously reported hydroxysumanene[21] by 135 mol % diethylaminosulfur trifluoride (DAST) in CH_2Cl_2 in 43% yield (Scheme 1). The fundamental properties of **1**

Scheme 1. Synthesis of 1-Fluorosumanene (1)

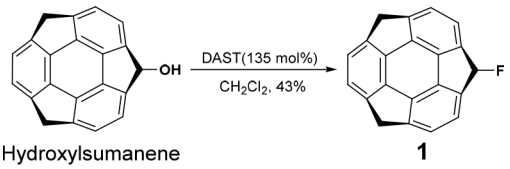

were confirmed by UV−vis spectroscopy and cyclic voltammetry (CV) experiments (Figures S1 and S2). The UV−vis spectrum of **1** showed similar absorption patterns of pristine **Sum** and other fluorosumanenes, showing an absorption at 276 nm with a broad peak at around 300 nm (Figure S1). These values are in between those of **F2-Sum** and **F6-Sum**.[25,26] The voltammogram of **1** in MeCN with tetrabutylammonium perchlorate as a supporting electrolyte showed a clear reduction peak (E_p^{red} = −1.81 V (vs Fc^0/Fc^+), Figure S2) which positively shifted compared with that of **Sum** (E_p^{red} = −2.49 V (vs Fc^0/Fc^+)).[31]

The thermodynamic relationship between $\mathbf{1}_{endo}$ and $\mathbf{1}_{exo}$ was clarified by theoretical calculation and ^{1}H NMR measuremens. The theoretical analysis operated at the B3LYP/6-311+G(d,p) level of theory indicated that $\mathbf{1}_{endo}$ is 0.67 kcal/mol more stable than $\mathbf{1}_{exo}$ and the bowl inversion energy of $\mathbf{1}_{endo}$ was 20.74 kcal/mol while $\mathbf{1}_{exo}$ was 20.06 kcal/mol (Figure 2). These

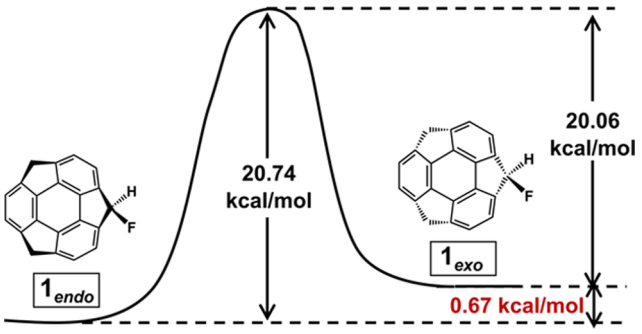

Figure 2. Structural and energetic difference between $\mathbf{1}_{endo}$ and $\mathbf{1}_{exo}$. All the calculation data were obtained at the B3LYP/6-311+G(d,p) level of theory.

calculation results agreed with the variable temperature ^{1}H NMR measurements in various solvents (Table 1). Regardless of the solvents and the temperature range, the *gem*-proton signal on the F-attached benzylic carbon of $\mathbf{1}_{endo}$ showed an intensity higher than that of $\mathbf{1}_{exo}$, appearing at a higher magnetic field (see Supporting Information). This observation strongly indicated that $\mathbf{1}_{endo}$ was the major component of the system. The van't Hoff plot based on the experimentally obtained *endo*:*exo* ratio at each temperature demonstrated no temperature range (193−373 K), in which the equilibrium relationship between $\mathbf{1}_{endo}$ and $\mathbf{1}_{exo}$ could be reversed (Tables 1 and S1, Figure S3). The thermodynamic parameters $\Delta_r H^{\ominus}$ and $\Delta_r S^{\ominus}$ displayed a notable compensatory correlation between enthalpy and entropy, suggesting a consistent inversion mechanism across all solvents (Figure S4).[32,33] It was

https://doi.org/10.1021/jacs.3c11311
J. Am. Chem. Soc. 2024, 146, 5224−5231

Table 1. *endo*:*exo* Ratio of 1 in CD_2Cl_2, Acetone-d_6, and DMF-d_7 at Various Temperatures[a]

	$\mathbf{1}_{endo}$:$\mathbf{1}_{exo}$		
temperature (K)	CD_2Cl_2	acetone-d_6	DMF-d_7
373			59:41
348			61:39
323			63:37
298	68:32	64:36	64:36
273	72:28	70:30	66:34
243	75:25	78:22	69:31
193	80:20	90:10	
Thermodynamic Parameter			
$\Delta_rH^{\ominus}$ (kJ mol^{-1})	2.7	7.4	2.5
$\Delta_rS^{\ominus}$ (J mol^{-1} K^{-1})	2.5	20	3.3

[a]All the samples were prepared in 1.5 mg/mL. Thermodynamic parameters $\Delta_rH^{\ominus}$ and $\Delta_rS^{\ominus}$ obtained via van't Hoff plot are also shown.

hypothesized that the positive entropy change, resulting from the flipping from a more crowded environment of $\mathbf{1}_{endo}$ due to the presence of solvent-interactive adjacent H atoms to a more F atom-exposed $\mathbf{1}_{exo}$ structure, serves as the primary driving force behind the bowl inversion process. Although the largest $\Delta_rS^{\ominus}$ value was obtained with acetone, the molecular size (van der Waals volume: CH_2Cl_2, 56.27 Å^3; acetone, 66.60 Å^3; DMF, 77.59 Å^3)[34] or polarity ($E_T(30)$: CH_2Cl_2, 40.7 kcal/mol; acetone, 42.2 kcal/mol; DMF, 43.2 kcal/mol)[35] did not explain the results, indicating simple consideration of solvent size and polarity does not solve this relationship, and more detailed and careful investigation of the whole bowl flipping process, including transition state through DFT calculation using cluster model of **1** and solvent molecule, is required,[36] which will be our future work.

The previous experiments confirmed that no conversion of the major species occurred in the diluted solution state. Nevertheless, considering the slight energetic difference between $\mathbf{1}_{endo}$ and $\mathbf{1}_{exo}$ is small (<1 kcal/mol), it is anticipated that the *endo*-favored condition is easily replaced by the *exo*-favored condition when perturbed by intermolecular interactions in a dense system, namely in the solid state. In this context, we next investigated how the *endo*:*exo* ratio changes in the solid state by crystallization conditions, such as solvent type and temperature. Single crystal preparation was performed by slow evaporation or vapor diffusion methods using three kinds of solvents, CH_2Cl_2, acetone, and DMF, with a temperature range from 193 to 323 K (Table 2). All the crystals were isostructural with **Sum** and already reported other fluorosumanenes,[25,26,29,30] trigonal *R*3*c* space group. In all the trials, the temperature effect was not significant, even though the entropic effect seemed to contribute to result in a slightly higher $\mathbf{1}_{endo}$ ratio at more than 298 K. Meanwhile, the *endo*:*exo* ratio of **1** in each crystal significantly differed depending on the type of crystallization solvent. Figure 3 shows the typical X-ray

Table 2. $\mathbf{1}_{endo}$:$\mathbf{1}_{exo}$ Ratio in a Single Crystal of 1 Prepared in CH_2Cl_2, Acetone, and DMF at Various Temperatures

	$\mathbf{1}_{endo}$:$\mathbf{1}_{exo}$		
temperature (K)	CH_2Cl_2	acetone	DMF
323		34:66	22:78
298	45:55	25:75	18:82
243	60:40	27:73	29:71
193	46:54	36:64	

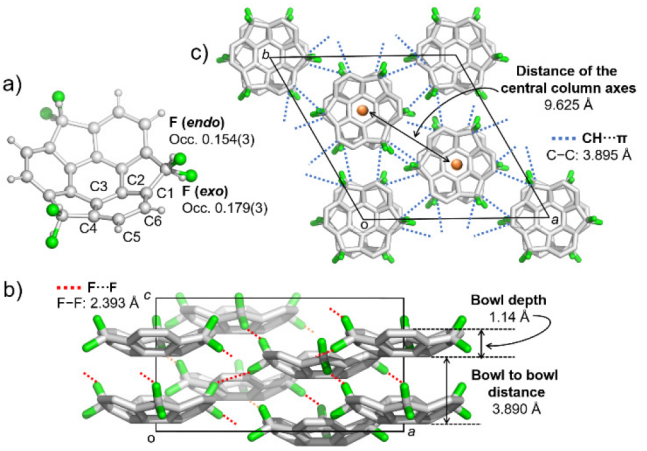

Figure 3. Representative crystal structure of **1**. The sample crystal was obtained by the slow evaporation method using CH_2Cl_2 at 193 K.

analysis results of the single crystals prepared from CH_2Cl_2 at 193 K. In the structure, we could find no solvent incorporation and observed that only one-third of the sumanene skeleton was independent. Within that, the two-electron densities dangling on the benzylic carbon were not equivalent, indicating the disordering of F atoms in a whole crystal. After refinement of the data, it was found that the occupancy factor of the two F atoms at the *endo* and the *exo* sides were 0.154(3) and 0.179(3), respectively; namely, the approximate $\mathbf{1}_{endo}$:$\mathbf{1}_{exo}$ ratio in the present crystal was 46:54 (Figure 3a). The bowl depth, defined by the vertical distance between the bottom hexagonal ring and the peripheral aromatic carbon, was 1.14 Å. This value was in between those of **Sum** (1.11 Å)[29] and **F2-Sum** (1.16 Å) (Figure 3b).[26]

In the crystal structure, $\mathbf{1}_{endo}$ and $\mathbf{1}_{exo}$ formed 1D columnar structure mainly stabilized by intracolumnar CH···π interactions between the benzylic C–H and π-plane of the sumanene skeleton and weak π–π interactions to give the bowl to bowl distance to be 3.890 Å (Figure 3b). All of the 1D-columns were connected through CH···π interactions (C–C: 3.895 Å) between benzylic carbon and neighboring aromatic carbons, probably with a slight contribution of CF···π and F···F interactions (2.393 Å) to stabilize the total packing structure with the distance of the central column axes to be 9.625 Å (Figure 3b,c). Notably, the *endo*:*exo* ratio difference did not affect the structural parameters much, supporting that the structural difference between $\mathbf{1}_{endo}$ and $\mathbf{1}_{exo}$ was well relaxed in the packing structures (Table S2). It is reasonable to assume that the slight structural and electronic difference between $\mathbf{1}_{endo}$ and $\mathbf{1}_{exo}$ was magnified in the crystal growing process via intermolecular interactions with solvents to achieve the formation of single crystals with such a variety of *endo*:*exo* ratios.

Such a biased *endo*:*exo* ratio in the crystal of **1**, coupled with the significant difference in dipole moments between $\mathbf{1}_{exo}$ and $\mathbf{1}_{endo}$, prompted us to apply **1** as a modifiable source of dielectric material. We tried to evaluate the dielectric response on the pelletized crystalline (**PC**) samples made from two kinds of crushed single crystals: recrystallized from DMF ($\mathbf{PC}_{DMF}$) or CH_2Cl_2 ($\mathbf{PC}_{CH_2Cl_2}$) ($\mathbf{1}_{endo}$:$\mathbf{1}_{exo}$ = 27:73 for $\mathbf{PC}_{DMF}$, 47:53 for $\mathbf{PC}_{CH2Cl2}$). Both samples underwent measurements

https://doi.org/10.1021/jacs.3c11311
J. Am. Chem. Soc. 2024, 146, 5224–5231

at several frequencies with the temperature range from 300 to 420 K (Figure 4) under N_2 atmosphere. There was a significant

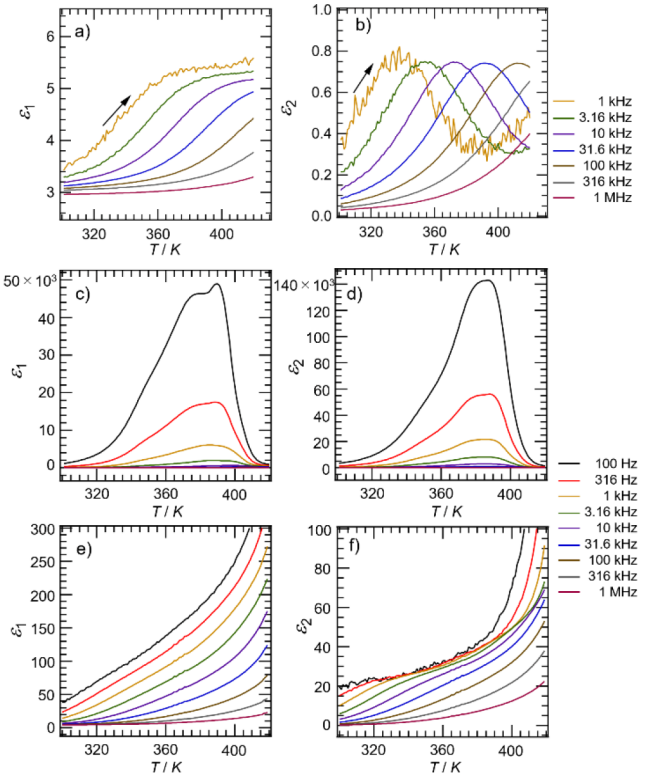

Figure 4. Temperature dependence of (a, c, e) the real part (ε_1) and (b, d, f) the imaginary part (ε_2) of the dielectric constant of $\mathbf{PC}_{DMF}$ (a, b) and $\mathbf{PC}_{CH2Cl2}$ (c–f) in compressed pellets measured at various frequencies. (e) and (f) represent the 2nd sweep results.

difference in the dielectric properties depending on the *endo*:*exo* ratio. In the case of $\mathbf{PC}_{DMF}$, both real (ε_1) and imaginary (ε_2) parts of the dielectric constant were enhanced above ~360 K at 1 MHz, with a Debye-type dielectric relaxation (Figure 4a,b). This phenomenon was quite similar to that of already reported **F2-Sum**,[26] indicating that the in-plane directional thermal vibration of polarized $\mathbf{1}_{exo}$ worked as the main contributor to the dielectric response. The $\ln(\tau)-T_{p1}^{-1}$ plots of $\mathbf{PC}_{DMF}$ indicated a linear correlation (Figure S5), where T_{p1} is the dielectric ε_1-peak and the τ-value is the relaxation time of the inverse of the measured *f*-values of $\tau = 1/(2\pi f)$. The activation energy for the thermally activated motion of $\mathbf{PC}_{DMF}$ was evaluated to be E_a = 70 kJ/mol, comparable to previously reported **F2-Sum** and other reported π-planar organic dielectrics (Figure S5).[37,38] On the contrary, $\mathbf{PC}_{CH2Cl2}$ showed significantly high dielectric constants as a simple organic molecule even after carefully drying up the possibly containing solvents. After the first heating, the dielectric constant decreased significantly (Figure 4c–f). Based on the experimental results, considerable structural relaxation was expected to occur at high temperatures, leading to a more stabilized structure in which the thermally activated motion of $\mathbf{1}_{exo}$ is strongly prohibited.

Regarding utilizing the functional molecules, it is a significant benefit that just a change in crystallization solvent gives a substantial property difference. To obtain more profound insight into how each conformer and solvent contribute to the obtained results, we first conducted DFT calculations to investigate how the intermolecular interactions involved in the crystallization process of **1** affect the final $\mathbf{1}_{endo}$:$\mathbf{1}_{exo}$ ratio in the single crystal of **1**. Our analysis employed a simple dimer model of $\mathbf{1}_{endo}$ and $\mathbf{1}_{exo}$ to explore the most stable conformer and stacking order. We focused on evaluating the interaction energies between the upper and bottom sides of **1**s in the model. Here, interdimer interactions were not considered as intracolumnar interactions were approximately 10 times stronger than intercolumnar ones, especially for sumanene derivatives that pack in the *R*3*c* space group.[27] The dimer model preparation was prepared by optimizing $\mathbf{1}_{endo}$ and $\mathbf{1}_{exo}$ at the ωb97XD/6-311+G(d,p) level of theory, with the bowl-to-bowl distance to be 3.9 Å and a rotation angle θ of F-attached benzylic carbons set to 60° or 180° (Figure 5). It

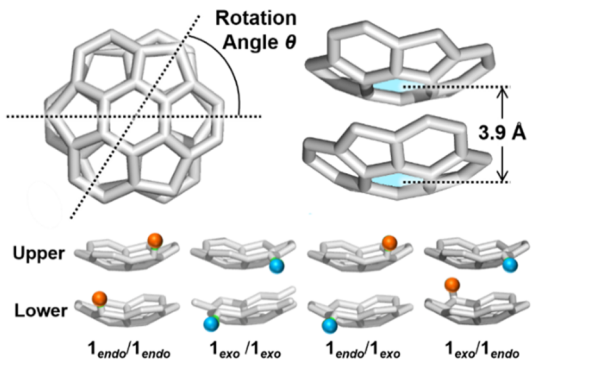

Upper/Lower	Interaction Energy (kcal/mol)[a]	
	60°	180°
$\mathbf{1}_{endo}/\mathbf{1}_{endo}$	−18.81	−18.35
$\mathbf{1}_{exo}/\mathbf{1}_{exo}$	−21.03	−21.34
$\mathbf{1}_{endo}/\mathbf{1}_{exo}$	−21.05	−21.10
$\mathbf{1}_{exo}/\mathbf{1}_{endo}$	−18.94	−18.92

a. Calculated at ωb97XD/6-311+G(d,p) level of theory.

Figure 5. Dimer model preparation and the resulting intermolecular energies based on the stacking species and order.

should be noted that all the possible stacking orders (upper or lower sides in the dimer) were considered. The simulation performed at the ωb97XD/6-311+G(d,p) level of theory clearly showed that the two dimers ($\mathbf{1}_{endo}/\mathbf{1}_{endo}$ and $\mathbf{1}_{exo}/\mathbf{1}_{endo}$), in which $\mathbf{1}_{endo}$ was placed at the bottom part of the stacking structure, were less stable (−18.35 to −18.94 kcal/mol) compared to the others ($\mathbf{1}_{exo}/\mathbf{1}_{exo}$ and $\mathbf{1}_{endo}/\mathbf{1}_{exo}$) with $\mathbf{1}_{exo}$ at the bottom position (−21.03 to −21.34 kcal/mol). These results were reasonable because the F atom of $\mathbf{1}_{endo}$ connected vertically to the bowl, leading to significant steric hindrance when another **1** came from the concave side. In contrast, the C–F bond on $\mathbf{1}_{exo}$ takes a somewhat in-plane direction of the bowl to avoid serious steric repulsion during stacking formation. These results explained that $\mathbf{1}_{exo}$ was more likely to be incorporated into the stacking column, especially when it approached the convex side. Indeed, the increment of $\mathbf{1}_{exo}$ ratio in all the crystals compared with the solution state data suggested that the above discussion is somewhat applicable to explaining the phenomena. However, the significant differences in the final *endo*:*exo* ratio in the crystalline state depending on the crystallization solvent indicated the presence of distinct solvent effects during the crystal growth, which assisted or interfered with introducing $\mathbf{1}_{exo}$ into the resulting crystal structure.

https://doi.org/10.1021/jacs.3c11311
J. Am. Chem. Soc. 2024, 146, 5224–5231

To illustrate the relationship between the solvent and the *endo*:*exo* ratio in the crystallization process, we applied molecular dynamics (MD) simulation considering three kinds of solvent systems: acetone, CH_2Cl_2, and DMF. All the molecules were modeled with a potential function based on the general Amber force field (GAFF) through DFT calculations at the B3LYP/6-31G(d,p) level for geometry optimization.[39,40] All the MD simulations were carried out with GROMACS 2020.6 in the *NPT* ensemble at 300 K, 1 bar for 30 ns (see Supporting Information for the simulation details).[41] We first investigated the effect of the solvent on the aggregation of $\mathbf{1}_{endo}$ and $\mathbf{1}_{exo}$. Three systems (100% population of each conformer or a 50:50 mixture of *endo* and *exo* conformers) were considered in the simulation. Note that there is no conversion between the *endo* and *exo* forms during the simulations. The concentration of **1** was 0.5 M at each run, and the population of the aggregates was examined. Here, we set the position of the center of mass on each conformer and defined the specific component as an "aggregate" when all the molecules are connected with a distance between centers of mass of 8 Å or less (see Supporting Information). The monomer population is larger in the order of DMF > CH_2Cl_2 > acetone for each conformer and the 50:50 mixture (Figure 6). Conversely, the

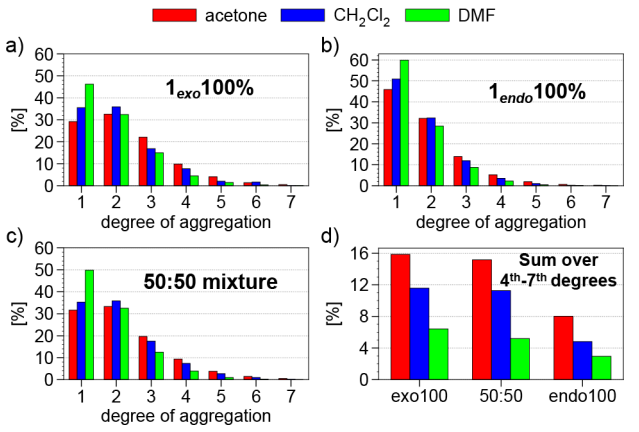

Figure 6. Aggregation state of **1** expressed as the % population of the number of molecules forming an aggregate with the degree of aggregation in the abscissae for (a) 100% $\mathbf{1}_{exo}$, (b) 100% $\mathbf{1}_{endo}$, and (c) 50:50 mixture of them in acetone, CH_2Cl_2, and DMF. The summed values over the degrees of aggregation of 4 or more are also shown in (d) to illustrate the dependence on the conformational states and solvents more clearly.

aggregation tendency is stronger with acetone > CH_2Cl_2 > DMF and is particularly suppressed in DMF. It is also seen in Figure 6 that the $\mathbf{1}_{endo}$ isomers are less likely to aggregate, indicating that the aggregation is more preferable for the $\mathbf{1}_{exo}$ form.

The relative preference of the $\mathbf{1}_{exo}$ and $\mathbf{1}_{endo}$ isomers in the monomeric and aggregates states are listed in Table 3. In acetone, for example, the monomeric $\mathbf{1}_{endo}$ and $\mathbf{1}_{exo}$ population is 57:43, implying the preference for the *endo* form when **1** is monomeric. This agrees with the experimental observation in Table 1, while Table 3 shows that more than half of **1** is in the *exo* form when the degree of aggregation exceeds 2. The tendency in CH_2Cl_2 was relatively close to the case in acetone, while in DMF, the $\mathbf{1}_{exo}$ population increment was not as steep as observed in acetone and CH_2Cl_2, and the average number was 3.3 even at the seventh degree of aggregation.

Table 3. Average Number of $\mathbf{1}_{exo}$ in Each Degree of Aggregation in Acetone, CH_2Cl_2, and DMF[a]

	degree of aggregation						
solvent	1	2	3	4	5	6	7
acetone	0.43	1.0	1.6	2.2	3.8	3.4	3.8
CH_2Cl_2	0.44	1.0	1.7	2.3	3.0	3.5	3.9
DMF	0.48	1.0	1.6	2.2	2.6	2.9	3.3

[a]The concentration of **1** in the system was 0.5 M, and the *endo*:*exo* ratio was 50:50.

We next analyzed the stacking manner of **1** in all of the aggregates, focusing on the neighboring pairs. A pair of **1** is counted as neighbors to each other when their center-of-mass distance is less than 8 Å. The MD simulation in acetone and CH_2Cl_2 revealed that the population of the $\mathbf{1}_{exo}/\mathbf{1}_{exo}$ combination became dominant as the degree of aggregation increased, while others with the *endo* form were on the decrease (Figure 7). This result matched the conclusion

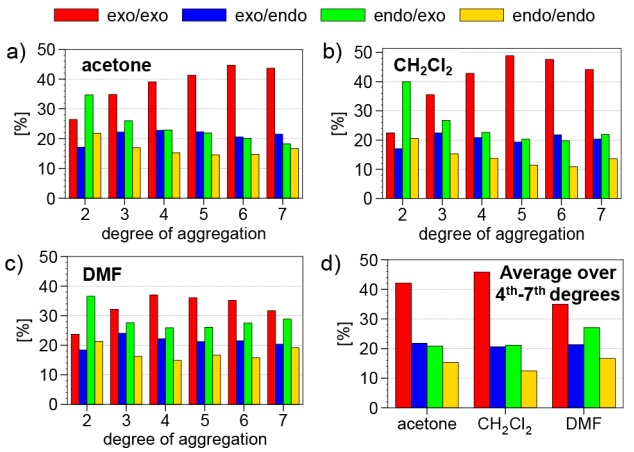

Figure 7. Population analysis data for neighboring pairs of $\mathbf{1}_{exo}/\mathbf{1}_{exo}$, $\mathbf{1}_{exo}/\mathbf{1}_{endo}$, $\mathbf{1}_{endo}/\mathbf{1}_{exo}$, and $\mathbf{1}_{endo}/\mathbf{1}_{endo}$ in various aggregates in (a) acetone, (b) CH_2Cl_2, and (c) DMF. The averaged data over the degrees of aggregation of 4 or more are shown in (d) to illustrate the dependence on the solvents more clearly. The definition of the neighboring pairs follows Figure 5.

obtained from the DFT calculation that $\mathbf{1}_{exo}$ positively contributed to the elongation of the stacks more than $\mathbf{1}_{endo}$. The same tendency was observed in the case of DMF, although the population of $\mathbf{1}_{exo}/\mathbf{1}_{exo}$ is smaller than those in the other two cases, in agreement with the smaller number for $\mathbf{1}_{exo}$ in Table 3.

The above discussion indicated that $\mathbf{1}_{exo}$ was more easily introduced in the aggregates than $\mathbf{1}_{endo}$, contributing to its elongation, and that aggregation is somehow suppressed in DMF. It should be noted, though, that the *endo* and *exo* conformers ratio is 50:50 in their mixture systems in MD. As shown in Table 1, the experimental *endo*:*exo* ratio is not 50:50, and this also affects the extent of *exo* propensity at recrystallization, as discussed next.

The energetic difference in Figure 1 was computed in a vacuum, and the *endo*:*exo* ratio is modified due to the solvation effect. This effect is quantified by the solvation free energy $\Delta\mu$ of a monomeric **1**, which is shown in Figures 8.[42,43] It is evident that the *exo* form interacts more favorably with each solvent than does *endo* and partially cancels the *endo*

https://doi.org/10.1021/jacs.3c11311
J. Am. Chem. Soc. 2024, 146, 5224−5231

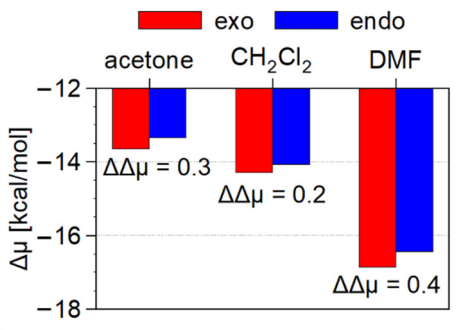

Figure 8. Solvation free energy $\Delta\mu$ of $\mathbf{1}_{endo}$ and $\mathbf{1}_{exo}$ in acetone, CH_2Cl_2, and DMF. $\Delta\Delta\mu = \Delta\mu(\mathbf{1}_{endo}) - \Delta\mu(\mathbf{1}_{exo})$ is noted in units of kcal/mol for each solvent.

preference in Figure 1. The extent of partial cancellation is stronger in the order of DMF > acetone > CH_2Cl_2, which means that the *exo* population is larger in this order when the recrystallization process starts. As discussed in Figure 7, on the other hand, the tendency for *exo* inclusion is more evident in acetone and CH_2Cl_2. With the combination of the two effects, accordingly, the *exo* population in the crystal is high with solvent DMF in Table 2 due to enhanced stability of the *exo* form at the outset of recrystallization, and it is high with acetone due to the higher inclusion efficiencies of $\mathbf{1}_{exo}$. Indeed, Table 3 and Figures 7 and 8 show for the solvent effects that the *exo* form is less favorably incorporated into aggregates when it is more strongly solvated. The energetic preference toward *exo* pairs in aggregates competes against that for the *exo* monomer at solvation, and the latter effect is more important than the former to determine the *exo* propensity at recrystallization. Accordingly, a guideline can be proposed that the crystal becomes richer with *exo* when the *exo*−solvent interactions are made stronger.

CONCLUSION

We successfully synthesized monofluorosumanene **1**, which is a diastereomeric mixture of $\mathbf{1}_{exo}$ and $\mathbf{1}_{endo}$ due to bowl inversion. Our experimental and theoretical investigations uncovered the energetic relationship among $\mathbf{1}_{exo}$, $\mathbf{1}_{endo}$ and solvent, enabling us to arrange the *endo*:*exo* ratio in the single crystals of **1** by the appropriate choice of the crystallization solvent. Throughout our project, it was found that the solvation made $\mathbf{1}_{exo}$ more stable, though it was not sufficient to reverse the intrinsic stability of $\mathbf{1}_{endo}$, resulting in a higher population of $\mathbf{1}_{endo}$ in the solution state. However, the sterically favorable structure of $\mathbf{1}_{exo}$ for aggregation facilitated the inversion of the *endo*:*exo* ratio in the solid state. Our DFT calculations and MD simulations played a pivotal role in understanding the underlying mechanisms, highlighting the critical impact of the solvation stabilization effect and the inclusion efficiency of $\mathbf{1}_{exo}$. Such an arrangeable *endo*:*exo* ratio of **1** realized the preparation of unique materials that exhibit entirely different dielectric responses. One showed the Debye type dielectric relaxation, while the other displayed a significantly high dielectric constant, all derived from the same molecule **1**, solely by changing the crystallization solvent. This significant achievement opens up new applications for the bowl inversion phenomenon in the curved-π molecules and highlights the remarkable potential of fluorosumanenes as energy materials.

ASSOCIATED CONTENT

Supporting Information

The Supporting Information is available free of charge at https://pubs.acs.org/doi/10.1021/jacs.3c11311.

Synthesis of **1**, ^{1}H NMR, ^{13}C NMR, and ^{19}F NMR charts of **1**, detailed experimental procedures, single crystal X-ray analysis details, molecular dynamics simulation detail, computational procedures with Cartesian coordinates, and supplemental figures and tables about optical and electrical properties of **1**, equilibrium details of **1** in each solvent, structural parameters of single crystal of **1**, and Arrhenius plot obtained from PC_{DMF} (PDF)

Accession Codes

CCDC 2288999−2289010 contain the supplementary crystallographic data for this paper. These data can be obtained free of charge via www.ccdc.cam.ac.uk/data_request/cif, or by emailing data_request@ccdc.cam.ac.uk, or by contacting The Cambridge Crystallographic Data Centre, 12 Union Road, Cambridge CB2 1EZ, UK; fax: +44 1223 336033.

AUTHOR INFORMATION

Corresponding Author

Yumi Yakiyama − *Division of Applied Chemistry, Graduate School of Engineering and Innovative Catalysis Science Division, Institute for Open and Transdisciplinary Research Initiatives (ICS-OTRI), Osaka University, Osaka 565-0871, Japan;* orcid.org/0000-0003-4278-2015; Email: yakiyama@chem.eng.osaka-u.ac.jp

Authors

Minghong Li − *Division of Applied Chemistry, Graduate School of Engineering, Osaka University, Osaka 565-0871, Japan*

Dongyi Zhou − *Division of Applied Chemistry, Graduate School of Engineering, Osaka University, Osaka 565-0871, Japan*

Tsuyoshi Abe − *Division of Applied Chemistry, Graduate School of Engineering, Osaka University, Osaka 565-0871, Japan*

Chisato Sato − *Graduate School of Engineering, Tohoku University, Sendai 980-8579, Japan*

Kohei Sambe − *Graduate School of Engineering, Tohoku University, Sendai 980-8579, Japan*

Tomoyuki Akutagawa − *Graduate School of Engineering, Tohoku University, Sendai 980-8579, Japan; Institute of Multidisciplinary Research for Advanced Materials (IMRAM), Tohoku University, Sendai 980-8577, Japan;* orcid.org/0000-0003-3040-1078

Teppei Matsumura − *Division of Chemical Engineering, Graduate School of Engineering Science, Osaka University, Toyonaka, Osaka 560-8531, Japan*

Nobuyuki Matubayasi − *Division of Chemical Engineering, Graduate School of Engineering Science, Osaka University, Toyonaka, Osaka 560-8531, Japan;* orcid.org/0000-0001-7176-441X

Hidehiro Sakurai − *Division of Applied Chemistry, Graduate School of Engineering and Innovative Catalysis Science Division, Institute for Open and Transdisciplinary Research Initiatives (ICS-OTRI), Osaka University, Osaka 565-0871, Japan;* orcid.org/0000-0001-5783-4151

Complete contact information is available at:

https://doi.org/10.1021/jacs.3c11311
J. Am. Chem. Soc. 2024, 146, 5224−5231

https://pubs.acs.org/10.1021/jacs.3c11311

Notes

The authors declare no competing financial interest.

■ ACKNOWLEDGMENTS

This work was supported by Grant-in-Aid for Scientific Research on Innovative Areas "π Space Figuration" (Grant JP26102002), Grant-in-Aid for Transformative Research Areas "Science of 2.5 Dimensional Materials" (Grants JP21H05232 and JP21H05233), "Hyper-Ordered Structures Sciences" (Grants JP21H05563 and JP23H04112), JSPS KAKENHI (Grants JP19H00912 and JP20H00400), and Dynamic Alliance for Open Innovation Bridging Human, Environment and Materials (Grants 20224023 and 20234025). The X-ray diffraction studies of one of the single crystal of **1** by synchrotron radiation were performed at BL02B1 of SPring-8 (Grant 2022A1330). The theoretical calculations were performed at the Research Centre for Computational Science, Okazaki, Japan (Grant 22-IMS-C068). We thank Prof. Gaku Fukuhara for the fruitful discussions about the solvation phenomena of **1**. Y.Y. is grateful for support from the program "Initiative for Realizing Diversity in the Research Environment", Osaka University. M.L. thanks the China Scholarship Council for support (Grants CSC 201708310115 and CSC 201908050056). N.M. is grateful to the Fugaku Supercomputer Project (Grants JPMXP1020230325 and JPMXP10-20230327) and the Data-Driven Material Research Project (Grant JPMXP1122714694) from the Ministry of Education, Culture, Sports, Science, and Technology.

■ REFERENCES

(1) Davey, R. J.; Schroeder, S. L. M.; ter Horst, J. H. Nucleation of Otganic Crystals-A molecular Perspective. *Angew. Chem., Int. Ed.* **2013**, *52*, 2166−2179.

(2) Gavezzotti, A.; Filippini, G.; Kroon, J.; van Eijck, B. P.; Klewinghaus, P. The Crystal Polymorphism of Tetolic Acid ($CH_3C{=}CCOOH$): A Molecular Dynamics Study of Precurosrs in Solution, and a Crystal Structure Generation. *Chem.—Eur. J.* **1997**, *3*, 893−899.

(3) Davey, R. J.; Blagden, N.; Righini, S.; Alison, H.; Quayle, M. J.; Fuller, S. Crystal Polymorphism as a Probe for Molecular Self-Assembly during Nucleation from Solutions: The Case of 2,6-Dihidroxybenzoic Acid. *Cryst. Growth Des.* **2001**, *1*, 59−65.

(4) Spitaleri, A.; Hunter, C. A.; McCabe, J. F.; Packer, M. J.; Cockroft, S. L. A ^{1}H NMR study of crystal nucleation in solution. *CrystEngComm* **2004**, *6*, 489−493.

(5) Parveen, S.; Davey, R. J.; Dent, G.; Pritchard, R. G. Linking solution chemistry to crystal nucleation: the case of tetrolic acid. *Chem.Commun.* **2005**, 1531−1533.

(6) Davey, R. J.; Dent, G.; Mughal, R. K.; Parveen, S. Concerning the Relationship between Structural and Growth Synthons in Crystal Nucleation: Solution and Crystal Chemistry of Calboxylic Acids As Revealed thorough IR Spectroscopy. *Cryst. Growth Des.* **2006**, *6*, 1788−1796.

(7) Chen, J.; Trout, B. L. Computational Study of Solvent Effects on the Molecular Self-Assembly of Tetrolic Acid in Solution and Implications for the Polymorph Formed from Crystallization. *J. Phys. Chem. B* **2008**, *112*, 7794−7802.

(8) Habgood, M. Solution and nanoscale structure selection: implications for the crystal energy landscape of tetrolic acid. *Phys. Chem. Chem. Phys.* **2012**, *14*, 9195−9203.

(9) Sullivan, R. A.; Davey, R. J.; Sadiq, G.; Dent, G.; Back, K. R.; ter Horst, J. H.; Toroz, D.; Hammond, R. B. Revealing the Roles of Desoluvation and Molecular Self-Assembly in Crystal Nucleation from Solution: Benzoic and *p*-Aminobenzoic Acids. *Cryst. Growth Des.* **2014**, *14*, 2689−2696.

(10) Gaines, E.; Maisuria, K.; Di Tommaso, D. The role of solvent in the self-assembly of *m*-aminobenzoic acid: a density functional theory and molecular dynamics study. *CrystEngComm* **2016**, *18*, 2937−2948.

(11) Hunter, C. A.; McCabe, J. F.; Spitaleri, A. Solvent effects of rrthe structures of prenucleation aggregates of carbamazepine. *CrystEngComm* **2012**, *14*, 7115−7117.

(12) Zeglinski, J.; Kuhs, M.; Khamar, D.; Hegarty, A. C.; Devi, R. K.; Rasmuson, Å. C. Crystal Nucleation of Tolbutamide in Solution: Relationship to Solvent, Solute Conformation, and Solution Structure. *Chem.—Eur. J.* **2018**, *24*, 4916−4926.

(13) Chai, Y.; Wang, L.; Bao, Y.; Teng, R.; Liu, Y.; Xie, C. Investigating the Solvent Effect on Crystal Nucleation of Etoricoxib. *Cryst. Growth Des.* **2019**, *19*, 1660−1667.

(14) Simões, R. G.; Melo, P. L. T.; Bernardes, C. E.; Heilmann, M. T.; Emmerling, F.; Minas da Piedade, M. E. Linking Aggregation in Solution, Solvation, and Solubility of Simvastatin: An Experimental and MD Simulation Study. *Cryst. Growth Des.* **2021**, *21*, 544−551.

(15) Burton, R. C.; Ferrari, E. S.; Davey, R. J.; Finney, J. L.; Bowron, D. T. The Relationship between Solution Structure and Crystal Nucleation: A Neutron Scattering Study of Supersaturated Methanolic Solutions of Benzoic Acid. *J. Phys. Chem. B* **2010**, *114*, 8807−8816.

(16) Joseph, A.; Rodrigues Alves, J. S.; Bernardes, C. E. S.; Piedade, M. F. M.; Minas da Piedade, M. E. Tautomer selection through solvate formation: the case of 5-hydroxynicotinic acid. *CrystEngComm* **2019**, *21*, 2220−2233.

(17) Nakamuro, T.; Sakakibara, M.; Nada, H.; Harano, K.; Nakamura, E. Capturing the Moment of Emergence of Crystal Nucleus from Disorder. *J. Am. Chem. Soc.* **2021**, *143*, 1763−1767.

(18) Fujii, S.; Ziatdinov, M.; Higashibayashi, S.; Sakurai, H.; Kiguchi, M. Bowl Inversion and Electric Switching of Buckybowls on Gold. *J. Am. Chem. Soc.* **2016**, *138*, 12142−12149.

(19) Sakurai, H.; Daiko, T.; Hirao, T. A Synthesis of Sumanene, a Fullerene Fragment. *Science* **2003**, *301*, 1878.

(20) Amaya, T.; Sakane, H.; Muneishi, T.; Hirao, T. Bowl-to-bowl inversion of sumanene derivatives. *Chem. Commun.* **2008**, 765−767.

(21) Higashibayashi, S.; Onogi, S.; Srivastava, H. K.; Sastry, G. N.; Wu, Y.-T.; Sakurai, H. Stereoelectronic Effect of Courved Aromatic Structures: Favoring the Unexpxcted *endo* Confomration of Benzylic-Substituted Sumanene. *Angew. Chem., Int. Ed.* **2013**, *52*, 7314−7316.

(22) Kuvychko, I. V.; Dubceac, C.; Deng, S. H. M.; Wang, X.; Granovsky, A. A.; Popov, A. A.; Petrukhina, M. A.; Strauss, S. H.; Boltalina, O. V. $C_{20}H_4(C_4F_8)_3$: A Fluorine-Containing Annulated Corannulene that Is a Better Electron Acceptor Than C_{60}. *Angew. Chem., Int. Ed.* **2013**, *52*, 7505−7508.

(23) Dubceac, C.; Sevryugina, Y.; Kuvychko, I. V.; Boltalina, O. V.; Strauss, S. H.; Petrukhina, M. A. Self-Assembly of Aligned Hybrid One-Dimensional Stacks from Two Complementary π-Bowls. *Cryst. Growth Des.* **2018**, *18*, 307−311.

(24) Haupt, A.; Lentz, D. Corranulenes with Electron-Withdrawing Substituents: Synthetic Approaches and Resulting Structural and Electronic Properties. *Chem.—Eur. J.* **2019**, *25*, 3440−3454.

(25) Schmidt, B. M.; Topolinski, B.; Higashibayashi, S.; Kojima, T.; Kawano, M.; Lentz, D.; Sakurai, H. The Synthesis of Hexafluorosumanene and Its Congeners. *Chem.—Eur. J.* **2013**, *19*, 3282−3286.

(26) Li, M.; Wu, J.; Sambe, K.; Yakiyama, Y.; Akutagawa, T.; Kajitani, T.; Fukushima, T.; Matsuda, K.; Sakurai, H. Dielectric response of 1,1-difluorosumanene caused by an in-plane motion. *Mater. Chem. Front.* **2022**, *6*, 1752−1758.

(27) Li, M.; Chen, X.; Yakiyama, Y.; Wu, J.; Akutagawa, T.; Sakurai, H. Tuning the dielectric response by co-crystallization of sumanene and its fluorinated derivative. *Chem. Commun.* **2022**, *58*, 8950−8953.

(28) Yakiyama, Y.; Li, M.; Sakurai, H. Fluorosumanenes as building blocks for organic crystalline dielectrics. *Pure Appl. Chem.* **2023**, *95*, 421−430.

(29) Sakurai, H.; Daiko, T.; Sakane, H.; Amaya, T.; Hirao, T. Structural Elucidation os Sumanene and Generation of Its Benzylic Anions. *J. Am. Chem. Soc.* **2005**, *127*, 11580−11581.

(30) Mebs, S.; Weber, M.; Luger, P. A.; Schmidt, B. M.; Sakurai, H.; Higashibayashi, S.; Onogi, S.; Lentz, D. Experimental electron density of sumanene, a bowl-shaped fullerene fragment; comparison with the related corannulene hydrocarbon. *Org. Biomol. Chem.* **2012**, *10*, 2218−2222.
(31) Zanello, P.; Fedi, S.; de Biani, F. F.; Giorgi, G.; Amaya, T.; Sakane, H.; Hirao, T. The electrochemical inspection of the redox activity of sumanene and its concave CpFe complex. *Dalton Trans.* **2009**, 9192−9197.
(32) Liu, L.; Guo, Q. Isokinetic Relationship, Isoequilibrium Relationship, and Enthalpy-Entropy Compensation. *Chem. Rev.* **2001**, *101*, 673−696.
(33) Pan, A.; Biswas, T.; Rakshit, A. K.; Moulik, S. P. Enthalpy-Entropy Compensation (EEC) Effect: A Recisit. *J. Phys. Chem. B* **2015**, *119*, 15876−15884.
(34) Zhao, Y. H.; Abraham, M. H.; Zissimos, A. M. Fast Calculation of van der Waals Volume as a Sum of Atomic and Bond Contributions and Its Application to Drug Compounds. *J. Org. Chem.* **2003**, *68*, 7368−7373.
(35) Reichardt, C. *Solvents and Solvent Effects in Organic Chemistry*; Wiley-VCH: Weinheim, Germany, 2003.
(36) Bruno, C.; Benassi, R.; Passalacqua, A.; Paolucci, F.; Fontanesi, C.; Marcaccio, M.; Jackson, E. A.; Scott, L. T. Electrochamical and Theoretical Investigation of Corannulene Reduction Processes. *J. Phys. Chem. B* **2009**, *113*, 1954−1962.
(37) Harada, J.; Yoneyama, N.; Sato, S.; Takahashi, Y.; Inabe, T. Crystals of Charge-Transfer Complexes with Reorienting Polar Molecules: Dielectric Properties and Order-Disorder Phase Transitions. *Cryst. Growth Des.* **2019**, *19*, 291−299.
(38) Harada, J.; Ohtani, M.; Takahashi, Y.; Inabe, T. Molecular Motion, Dielectric Response, and Phase Transition of Charge-Transfer Crystals: Acquired Dynamic and Dielectric Properties of Polar Molecules in Crystals. *J. Am. Chem. Soc.* **2015**, *137*, 4477−4486.
(39) Wang, J.; Wolf, R. M.; Caldwell, J. W.; Kollman, P. A.; Case, D. A. Development and testing of a general amber force field. *J. Comput. Chem.* **2004**, *25*, 1157−1174.
(40) Bayly, C. I.; Cieplak, P.; Cornell, W. D.; Kollman, P. A. A well-behaved electrostatic potential based method using charge restraints for deriving atomic charges: the RESP model. *J. Phys. Chem.* **1993**, *97*, 10269−10280.
(41) Abraham, M. J.; Murtola, T.; Schulz, R.; Páll, S.; Smith, J. C.; Hess, B.; Lindahl, E. GROMACS: High performance molecular simulations through multi-level parallelism from laptops to supercomputers. *SoftwareX* **2015**, *1−2*, 19−25.
(42) Matubayasi, N.; Nakahara, M. Theory of Solutions in the Energy Representation. II. Functional for the Chemical Potential. *J. Chem. Phys.* **2002**, *117*, 3605−3616.
(43) Sakuraba, S.; Matubayasi, N. ERmod: Fast and Versatile Computation Software for Solvation Free Energy with Approximate Theory of Solutions. *J. Comput. Chem.* **2014**, *35*, 1592−1608.

https://doi.org/10.1021/jacs.3c11311
J. Am. Chem. Soc. 2024, 146, 5224−5231